Implications of Sorption on Carbon Dioxide Sequestration in Gas Shales

K. Arunachalam, X. Fan
Institute for Materials and Processes, School of Engineering, The University of Edinburgh, Edinburgh, EH9 3JL, UK

Abstract

Gas shales are one of the potential sinks considered for carbon dioxide sequestration. Therefore further research on the importance of sorption on the carbon dioxide sequestration potential is highly topical. Experimentally measured maximum sorption capacity of carbon dioxide was about 15% higher than that of methane. Carbon dioxide also exhibited a higher affinity towards these shales as compared to methane. Reservoir simulation accounting for sorbed gas revealed that huff-and-puff injection is not expected to increase methane recovery after 5 years of production. Adsorption uptake is a more important parameter compared to adsorption in the evaluation of carbon dioxide storage potential. With increasing adsorption uptakes, a lower amount of carbon dioxide was injected into the reservoir for a given injection period. Therefore longer injection periods as compared to production periods are necessary for gas shales to be carbon neutral. Sorbed carbon dioxide stored in the reservoir was found to be highly stable even during methane production, and can, therefore, be expected to less susceptible to leakage compared to other carbon dioxide sequestration technologies.

Keywords: shale, carbon dioxide, adsorption, COMSOL, experiment

1 Introduction

Carbon Capture and Storage has been identified as a key technology in several energy scenarios that meet the global emissions target set by the IPCC [1]. Shales have been identified as one of the potential reservoirs for carbon dioxide sequestration [2,3]. However, the impact of sorption on the potential of gas shales to store carbon dioxide in the reservoir is not well investigated.

Conventional reservoirs considered for carbon dioxide sequestration store the gas through either through capillary mechanism or through a solution mechanism. However, in gas shales, carbon dioxide is also stored through the adsorption mechanism. This could potentially result in a significant increase in the total carbon that could be stored in shales, and therefore needs further investigation before commercial deployment.

It is now well understood that nearly 20-80% of the total methane stored in shales is in an adsorbed state [4]. However, only 0.2% of the total sorbed gas is produced from the reservoir after primary recovery [5]. This is because adsorption in shales is controlled by Type I isotherms [6]. Several researchers have indicated that carbon dioxide in shales also follows a Type I isotherm [7]. It is also well understood that shales have a higher affinity to carbon dioxide typically adsorbing nearly 1.5 times the amount of carbon dioxide as it does methane [2,7–9]. This suggests that sorption in shales could significantly contribute to its carbon sequestration potential. However, given the importance of this phenomenon, further study is warranted in the context of how sorption affects actual carbon dioxide sequestration mechanisms in the reservoir.

This study presents methane and carbon dioxide isotherms on Lothian shales at 45 ^{o}C. The adsorption data is then integrated into a Finite Element reservoir simulation in COMSOL that allows us to study the behaviour of these fluids in a 2D system, with particular emphasis on the impact of sorption for carbon dioxide sequestration and enhanced hydrocarbon recovery.

2 Methodology

2.1 Porosity and Permeability

Bulk volume was measured by water immersion of shale samples previously saturated with water [10]:

$$V_{b,sp} = \frac{w_{water\ displaced}}{998.203 * w_{sh}} \quad (1)$$

Where $V_{b,sp}$ is the bulk volume. Grain volume was measured using He gas expansion [11]:

$$V_{g,sp} = \frac{(P_c - P_e) * V_r}{(P_e - P_i) * w_{sh}} \quad (2)$$

Where $V_{g,sp}$ is the grain volume, P_c is charge pressure, P_i is initial pressure, P_e is equilibrium pressure. V_R is reference cell volume, and w_{sh} is sample weight. Porosity was then calculated as follows [11]:

$$\phi = \frac{V_{b,sp} - V_{g,sp}}{V_{b,sp}} \quad (3)$$

Where ϕ is the shale porosity. Permeability was calculated from the early transient pressure data during He expansion [12]. Brent's algorithm for root finding is used to find out the permeability of the shale [13].

2.2 Adsorption

Sorption was measured in a high-pressure manometric rig [5]. The amount adsorbed was calculated injecting fixed amounts of the adsorptive into the sample cell [14]. Equilibrium was assumed when the rate of sorption per hour fell below an order of magnitude of the total sorption in a pressure step.

$$q_e = \frac{n_{injected} - n_{current}}{w_{sh}} \quad (4)$$

Excess sorption was converted to absolute sorption by assuming a surface coverage mechanism as shown in Equation (5) [15]. The adsorbed phase density of methane and carbon dioxide were assumed to be 26300 mol/m^3 and 21100 mol/m^3 respectively [5].

$$q_a = \frac{q_e}{1 - \frac{\rho_g}{\rho_{ads}}} \quad (5)$$

Where q_a is absolute sorption, q_e is excess sorption, ρ_g is gas-phase density, and ρ_{ads} is adsorbed phase density. Adsorbed phase density is assumed to be equal to the liquid phase density at saturation point [16].

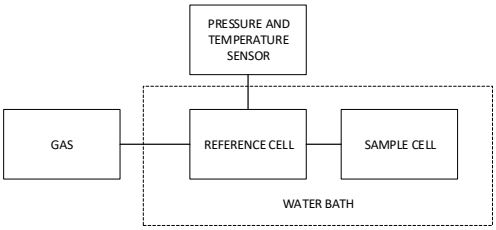

Figure 1 Manometric Rig from [5]

2.3 Langmuir Isotherm Model

The Langmuir isotherm is widely used to characterize Type I isotherms in shales [17]. It also offers several advantages over other isotherms used to characterize Type I isotherms, by offering thermodynamically consistent behaviour at low and high pressures [18].

$$q_a = q_L \frac{b_L \rho_g}{1 + b_L \rho_g} \quad (6)$$

The first derivative of the Langmuir isotherm to gas phase concentration is the adsorption uptake and is calculated as follows:

$$K_a = \rho_s q_L \frac{b_L}{\left(b_L \rho_g + 1\right)^2} \quad (7)$$

Where q_L is Langmuir adsorbed, b_L is Langmuir affinity, ρ_s is shale density.

2.4 Numerical Simulation

Reservoir model shown in Figure *2* is considered. The producing well and fractures are perpendicular to each other. This is difficult to study owing to complex geometries and the lack of understanding on fracture geometries [19]. Considering the symmetry of the model along the wellbore and the fractures, a smaller Simulated Reservoir Volume is used in this study and the FEM meshing is presented in Figure *3*. Studying gas flow in this area should give us an idea of the gas flow in the larger reservoir.

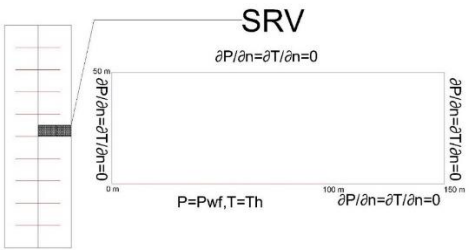

Figure 2 Reservoir model from [5]

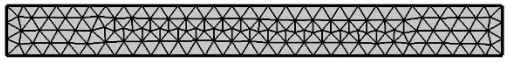

Figure 3 FEM Meshing

The general mass diffusion equation is modified to include sorption for this study [5].

$$\phi \frac{\partial \boldsymbol{\rho_g}}{\partial t} + (1-\phi)\frac{\partial \boldsymbol{\rho_a}}{\partial t} + \nabla\left(\frac{\boldsymbol{\rho_g k}}{\boldsymbol{\mu}}.\nabla \boldsymbol{P}\right) = Q \quad (8)$$

Where ρ_g is free gas density, ρ_a is sorbed gas density, k is permeability, μ is viscosity, and Q is production or injection. The above equation contains a correction term for the amount adsorbed in the shale matrix and can also be represented more canonically as:

$$\frac{\partial \boldsymbol{\rho_g}}{\partial t} + \nabla\left(\frac{\boldsymbol{k}}{\boldsymbol{\mu}(\phi+(1-\phi)\,\boldsymbol{K_a})}.\nabla \boldsymbol{P}\right) = Q \quad (9)$$

In this representation, sorption affects diffusion. Higher sorption uptakes can be expected to reduce the effective diffusion in shale. The Langmuir isotherm is used in COMSOL to model adsorption. This is preferred over other adsorption models as besides providing a good fit, it has consistent thermodynamic behaviour across the whole pressure range considered in shale reservoir simulation. Other isotherms such as the Freundlich model, does not have a monolayer volume at high pressures, or a linear sorption region at low pressures. Since methane production occurs in the monolayer region, and carbon dioxide sequestration occurs in the linear region, these are serious drawbacks in reservoir simulation. Further complexities arising due to real gas behaviour and relative permeabilities are ignored in this study. Surface diffusion effects are also neglected. This allows us to isolate the effects of sorption on the behaviour of gases in the reservoir. For readers interested in these effects, other studies in the literature are available [3]. Model parameters are summarised in Table *1*.

Boundary conditions are summarised in Figure *2*. Assuming an ideal fracture, a constant pressure boundary was implemented along the fracture [20]. It was assumed that the wellbore was perforated only along the fracture, and therefore gas flow into the wellbore along the matrix is 0. Owing to symmetries, all other boundaries are also 0. Smaller mesh size and a shorter time step were also considered without any changes to the resulting solution. The MUMPS solver was used in COMSOL to obtain the solution. Equation (8) along with the above-mentioned conditions was solved in COMSOL using the Transport of Diluted Species module for further analysis.

Table 1 Simulation Parameters

Parameter	Symbol	Value	Units
Porosity	ϕ_m	0.05	-
Permeability	k	4.99 x 10^{-22}	m^2
CH_4 viscosity	μ_m	11.71 x 10^{-6}	$Pa\ s$
CO_2 viscosity	μ_c	15.9 x 10^{-6}	$Pa\ s$
Shale density	ρ_s	2870	kg/m^3
Reservoir height		100	m
Reservoir width		10	m
Fracture height		80	m
Initial pressure		200	bar
Temperature		45	^0C
Well pressure		30	bar
Injection pressure		200	bar

3 Results

3.1 Experimental Characterization

Figure 4 plots the experimental pressures obtained during isotherm characterization. About 24 hours were required to characterize each isotherm. It can also be seen that lower pressure steps require longer equilibrium times as compared to higher pressure steps in general and that carbon dioxide isotherms require longer equilibrium times as compared to methane isotherms. The calculated isotherms from these experiments are plotted in Figure 5 and adsorption uptakes are plotted in Figure 6. Both the methane and carbon dioxide isotherms are Type I and are well characterized by Langmuir isotherms with an R-Squared value of over 0.99. Langmuir volume for methane and carbon dioxide were calculated as 0.36 mol/kg and 0.41 mol/kg respectively. Langmuir affinity constants

were calculated as 5.91 10^{-4} m^3/mol and 1.11 10^{-3} m^3/mol respectively. Given that carbon dioxide has both a higher adsorption capacity and a higher affinity to shales as compared to methane, carbon dioxide sequestration in shales could be theoretically feasible.

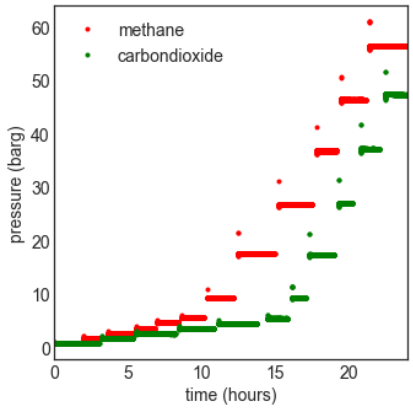

Figure 4 Experimental pressures obtained from manometric rig during sorption characterization

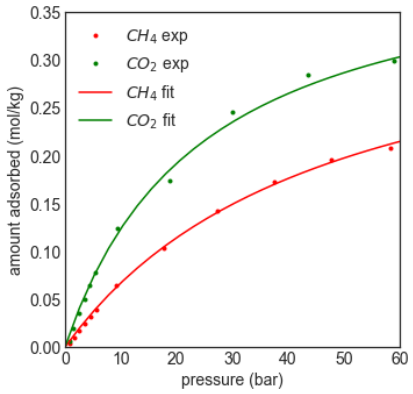

Figure 5 Adsorption isotherms with Langmuir fit

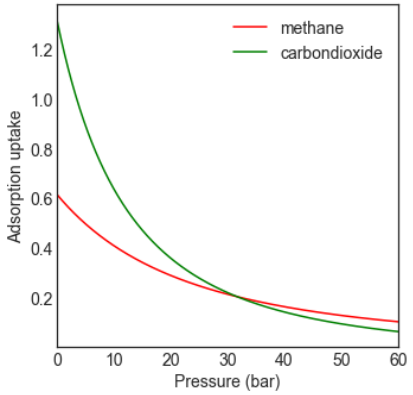

Figure 6 Adsorption uptake based on Langmuir fits

3.2 Reservoir Simulation

Figure *11* plots methane produced and carbon dioxide sequestered in the reservoir against time. Two simulation cases are considered. In the first case, methane is produced for 10 years, and carbon dioxide is produced for the next 10 years. The second case consists of 4 cycles of 5 years each – methane production, carbon dioxide injection, methane production, and carbon dioxide injection. It can be seen from Figure *11* that carbon dioxide is injected at a much slower rate than methane. This can be explained as carbon dioxide adsorption uptake is significantly higher than the methane adsorption uptake. Since with increasing adsorption uptakes, longer periods are required to achieve the same amount of mass transfer [21], this behaviour is to be expected. Because of this behaviour, longer injection times would be required inject the same amount of carbon into the reservoir as was originally produced. However, after 10 years of injection, it was possible to reduce the carbon cost of shale gas by almost 70%.

From Figure 7 and Figure 8, it is possible to see that there is a significant amount of desorption happening when methane production is halted and carbon dioxide injected. However, from Figure *11*, huff and puff carbon dioxide injection is not sufficient to increase methane recovery at the end of 15 years. These results are in agreement with other studies on carbon dioxide enhanced recovery [3]. This suggests that further production technologies may be required to increase the methane recovery rate from the reservoir.

From Figure 7 and Figure 9, it can be seen that the ratio of sorbed gas contributing to carbon dioxide sequestration is almost 5 times the ratio of sorbed gas that contributes to methane production. This trend is also reflected in Figure *11* where the total sorbed carbon dioxide stored in the reservoir after the injection period is higher than the total sorbed methane that is produced despite the opposite phenomenon being observed for total amounts.

We would finally like to draw the reader's attention to the second methane production cycle

in Figure *11*. There is a net loss of carbon dioxide sequestered as it would be expected with a flowing wellbore. However, the amount of sorbed carbon dioxide displaced has remained constant. This provides strong evidence that sorbed carbon dioxide is highly stable and less susceptible to carbon leakage over long periods. Given that carbon leakage is a strongly contested issue in the research community [1], sorbed carbon dioxide storage in gas shales could be an excellent way to take CCS technologies forward.

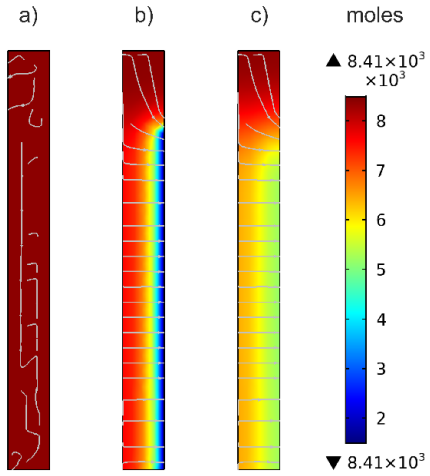

Figure 7 Total methane distribution. Subfigures a – 0 years; b – 10 years; c – 20 years.

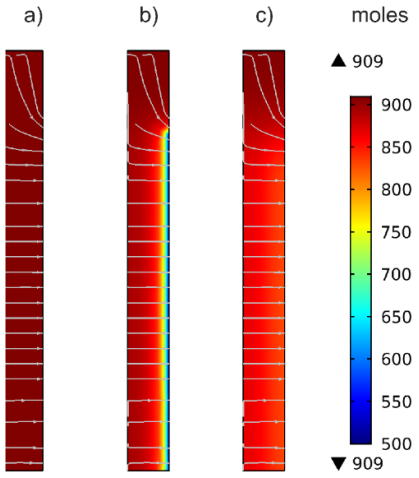

Figure 8 Adsorbed methane distribution.

Subfigures a – 0 years; b – 10 years; c – 20 years.

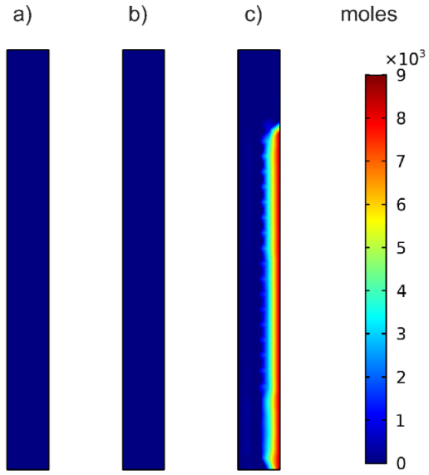

Figure 9 Total carbon dioxide. Subfigures a – 0 years; b – 10 years; c – 20 years.

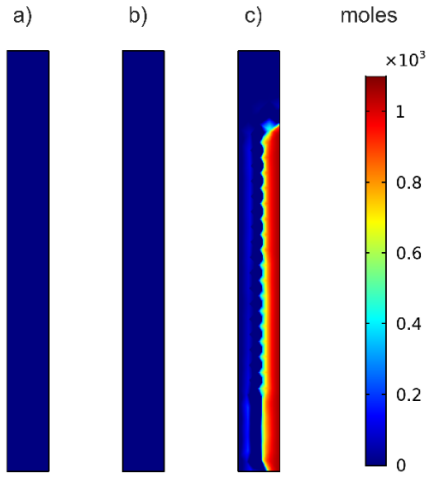

Figure 10 Adsorbed carbon dioxide. Subfigures a – 0 years; b – 10 years; c – 20 years.

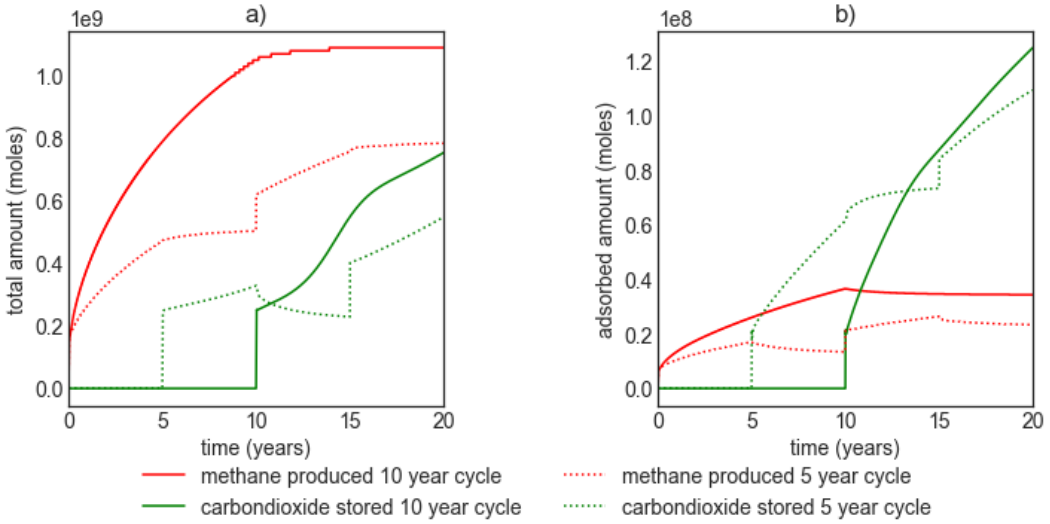

Figure 11 Methane production and carbon dioxide sequestration Estimates. Subfigure a plots total gas. Subfigure b plots adsorbed gas.

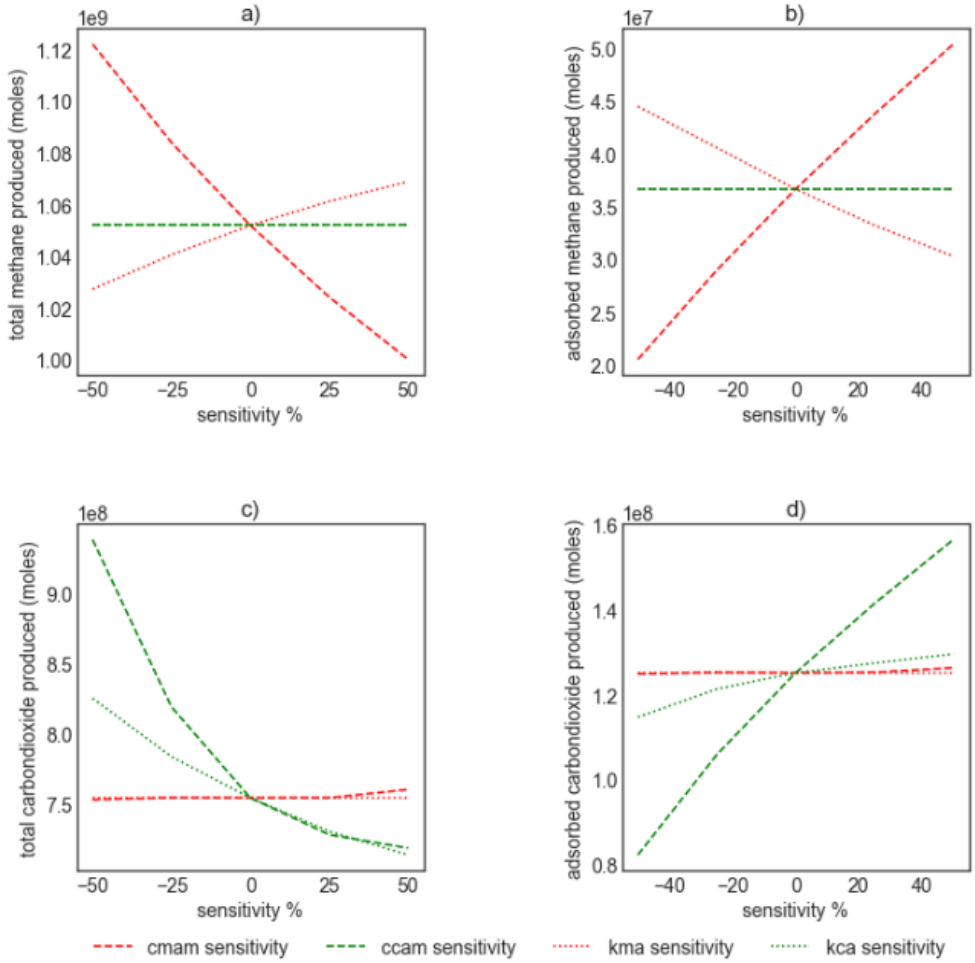

Figure 12 Sensitivity of adsorption parameters on methane production and carbon dioxide sequestration

3.3 Sensitivity Analysis

Figure 12 plots the sensitivities of adsorption parameters on total and sorbed methane produced, and total and sorbed carbon dioxide sequestered in the reservoir. It can be seen that maximum sorption capacities are inversely correlated with total methane production and carbon dioxide sequestered in agreement with previous results [21]. However, adsorption affinities are positively correlated. This trend is reversed for sorbed methane produced and carbon dioxide sequestered.

These results suggest that longer production and injection times would be necessary to realise a similar amount of mass transfer for shales with high adsorption uptakes.

4 Conclusion

Carbon dioxide sequestration potential of gas shales was analysed using experimental and simulation techniques. Both adsorption and adsorption uptake parameters strongly influence carbon dioxide sequestration potential of shales. Huff and puff carbon dioxide injection did not increase methane recovery from the reservoir. Longer periods were required for carbon dioxide sequestration as compared to methane production toa achieve a similar mass transfer.

References

1 Mathieu, P. in *ECOS 2006* - (2006)
2 Nuttall, B. C. *et al.* (University Of Kentucky Research Fdn, 2005)
3 Liu, F. *et al. Int. J. Greenh. Gas Control* 17, 111–126 (2013)
4 Schettler Jr, P. D. *et al.* in *SPE Eastern Regional Meeting* (Society of Petroleum Engineers, 1991)
5 Arunachalam, K. *et al. J. Nat. Gas Sci. Eng.* 79, 103318 (2020)
6 Rouquerol, J. *et al.* (Academic press, 2013)
7 Heller, R. *et al. J. Unconv. Oil Gas Resour.* 8, 14–24 (2014)
8 Merey, S. *et al. J. Nat. Gas Sci. Eng.* 36, 1087–1105 (2016)
9 Rani, S. *et al. Journal of Petroleum Science and Engineering* 175, (2019)
10 Kuila, U. *et al. Fuel* 117, 1115–1129 (2014)
11 RP40, A. *Feb* (1998)
12 Cui, X. *et al. Geofluids* 9, 208–223 (2009)
13 Brent, R. P. *Comput. J.* (1971)
14 Rouquerol, J. *et al. Pure Appl. Chem.* 66, 1739–1758 (1994)
15 Wang, Y. *et al. Fuel* 172, 301–309 (2016)
16 Pini, R. *Microporous Mesoporous Mater.* 187, 40–52 (2014)
17 Langmuir, I. *J. Am. Chem. Soc.* 40, 1361–1403 (1918)
18 Do, D. D. (1998)
19 Warren, J. E. *et al. Soc. Pet. Eng. J.* 3, 245–255 (1963)
20 Teng, T. *et al. J. Nat. Gas Sci. Eng.* 34, 1174–1190 (2016)
21 Arunachalam, K. *et al.* (2020)